

ANALYSIS OF HELIOSEISMIC WAVE FIELDS TO EXAMINE HORIZONTAL STRUCTURES

K.A. Julien¹, D.O. Gough^{2,3} and J. Toomre³

¹High Altitude Observatory, National Center for Atmospheric Research, Boulder, Colorado, USA

²Institute of Astronomy, University of Cambridge, Cambridge, UK

³Joint Institute for Laboratory Astrophysics, University of Colorado, Boulder, Colorado, USA

1. ABSTRACT

We present and evaluate a preliminary inversion procedure for carrying out a local area analysis on simulated oscillation data to deduce two-dimensional subsurface structures in the horizontal, representative of thermal variations, potentially as function of depth.

2. INTRODUCTION

The advent of nearly continuous observations from GONG, and similar higher resolution data from the SOI-MDI instrument on SOHO, offers major opportunities to study solar wave fields in appreciable detail. An important goal of helioseismology is to detect coherent horizontal structures that may be present within the highly turbulent solar convection zone. Temperature structures and subsurface flows may be sought by analysing distortions of the acoustic wave field which arise from variations in the sound speed and differential advection effects. Preliminary results were presented by Gough et al. (1992, 1993), showing that one-dimensional simulated acoustic wave-train data obtained by assuming propagation in just one horizontal direction can be inverted to reveal local variations in sound speed. With this procedure, one-dimensional structure was recovered by extracting the phase distortions of the wave-trains using one-dimensional Hilbert transforms followed by the use of the JWKB approximation. However, that model is highly simplified, for it neglects both lateral scattering by two-dimensional inhomogeneity and interference between waves of the same frequency propagating in different directions. Analysing the importance of these effects using artificial oscillation data requires a non-trivial extension to two-dimensional wave fields propagating on an inhomogeneous background.

3. THE WAVE EQUATION

The problem addressed is the evaluation of an inversion procedure that utilizes information gained from the phase distortion occurring in artificially generated acoustic wave to determine subsurface thermal structure. These distortions in the acoustic wave fields would naturally arise as direct consequence of convective motions in the solar interior. We restrict our attention to acoustic modes of high degree. For in that case acoustic oscillations are

trapped in a shallow wave guide just beneath the photosphere: the base of the trapping region being at depth $z_t = (2n + 3)l^{-1}R$, where n and l are the order and degree of the mode and R is the radius of the sun. Because the trapping region is shallow the effects of curvature are neglected to leading order. Furthermore subsurface oscillations are assumed adiabatic and to occur within the plane unstratified atmosphere, thus gravity $g = 0$ and the pressure p is a constant satisfying $\nabla p = 0$.

Knowledge of thermal inhomogeneity in the atmosphere, characterised by local variations in density, is obtained via the determination of the sound speed c , through the relation

$$c^2(x, y, z) = \gamma p / \rho(x, y, z),$$

where γ is the adiabatic exponent (assumed constant) and $\rho(x, y, z)$ is the density. The governing equations describing acoustic wave propagation through such an inhomogeneous background are the linearised Navier-Stokes equations (neglecting dissipation)

$$\partial_t \rho' = -\nabla \cdot (\rho \mathbf{u}), \quad \partial_t p' = c^2(\partial_t \rho' + \mathbf{u} \cdot \nabla \rho)$$

$$\partial_t \mathbf{u} = -\frac{1}{\rho} \nabla p'.$$

The variable \mathbf{u} and the primed quantities respectively denote the velocity and thermodynamic fluctuations about the background state $(p, \rho(x, y, z))$ due to wave motions. These are considered small in their amplitudes thus nonlinear terms are neglected. Background inhomogeneities in velocity arising from convective motions are neglected (this will be the subject of a future publication). Elimination of u, ρ' together with the change of variable $\Psi = \rho^{-1/2} p'$ leads to a single wave equation, namely,

$$\left[\nabla^2 - \frac{\omega_c^2}{c^2} \right] \Psi = \frac{1}{c^2} \partial_{tt} \Psi, \quad (1)$$

where

$$\frac{\omega_c^2}{c^2}(x, y, z) = \frac{\kappa^2}{4} + \frac{1}{2} \nabla \cdot \kappa \quad \text{with} \quad \kappa = -\nabla \rho / \rho.$$

ω_c denotes the cut-off frequency. The wave variable Ψ may be interpreted as the linear superposition of high-degree acoustic oscillations confined to propagate within the shallow wave guide directly beneath the photosphere. Such a superposition constitutes the discrete spectrum of modes in frequency (ω) and wavenumber (k) space. The depth of the wave guide for a given mode is inversely

proportional to the square of the frequency at fixed n :

$$z_t \propto \left[\frac{(2n+3)}{\omega} \right]^2$$

. Therefore, given that wave propagation occurring within the shallow atmosphere is essentially horizontal implies that modes of different frequency ω sample different depths. Specifically, the horizontal structure at depth $z = z_*$ may be investigated by Fourier transforming (1) in time t and isolating the normal modes $\Psi = \hat{\Psi}(x, y; \omega_*)e^{-i\omega_*t}$ with associated frequency ω_* . Ψ then satisfies the Helmholtz equation

$$[\nabla_{\perp}^2 + K^2]\Psi = 0, \quad \text{with} \quad K^2 = \left[\frac{\omega_*^2 - \omega_{\perp c}^2}{c_{\perp}^2} \right].$$

∇_{\perp}^2 is the horizontal Laplacian operator. This equation denotes the starting point from which artificial acoustic waves are generated. Specifically, variations in the local wavenumber K is a function of the horizontal inhomogeneity in the medium (due to sound speed variations) that are assumed weak (i.e. $O(\varepsilon)$ with $\varepsilon \ll 1$). Thus, we write

$$K^2 = k^2 \frac{(1 + \varepsilon f(x, y))^2}{\langle (1 + \varepsilon f(x, y))^2 \rangle}, \quad (2)$$

where $\langle \rangle$ denotes the horizontal average and $k^2 = \langle K^2 \rangle$ defines a characteristic wave number associated with the mean background $\langle \rho \rangle$ at frequency ω_* , and f defines the weak variation, which for the purposes of this numerical investigation is considered a known function to be specified (Figure 1).

4. METHODOLOGY AND SOLUTION

The solution Ψ for a given $K(x, y; \omega_*)$ is sought to provide the artificial wave data for the inversion procedure. Given the ansatz (2) the problem is treated by perturbation theory, using $\varepsilon \ll 1$ as the order parameter in the expansion

$$\Psi = \Psi_0 + \varepsilon \Psi_1 + \dots$$

This gives the following hierarchy of linear partial differential equations to solve

$$\begin{aligned} O(\varepsilon^0) : \nabla_{\perp}^2 \Psi_0 + k^2 \Psi_0 &= 0, \\ O(\varepsilon^1) : \nabla_{\perp}^2 \Psi_1 + k^2 \Psi_1 &= G =: -2k^2 \Psi_0 f, \quad \dots \end{aligned} \quad (3)$$

The solution to the zeroth-order problem is known and given by a specified superposition of n -plane waves

$$\Psi_0 = \sum_n A_n \cos(\mathbf{k} \cdot \mathbf{x} + \delta_n), \quad |\mathbf{k}| = k.$$

This may be interpreted as the undistorted component of the acoustic wave field propagating through the mean background $\langle \rho \rangle$; A_n and δ_n represent the constant amplitude and phase of the individual wave components. The solution to the first-order inhomogeneous wave equation Ψ_1 then gives the scattered wave component which accounts for the distortion of the plane waves by the weak inhomogeneity $f(x, y)$. As a further simplification

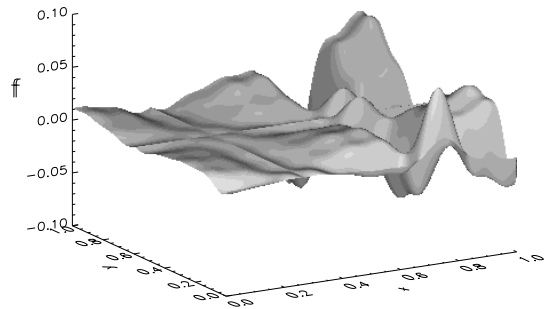


Figure 1. Sample variation $f(x, y)$ in the local wavenumber K due to variations in sound speed c .

the scattered wave solution is constrained such that no wave generation or decay occur within a specified observation region R , thus $f(x, y) \in \mathfrak{R}$, implying that the local wavenumber K is real. This is imposed by a radiation condition that forces all scattered waves to be outward propagating at the boundary δR . In the following analysis no higher-order terms in the expansion have been included.

We find, for numerical simplicity, that the application of a radiation boundary conditions demands that the computational domain be a circular geometry with $R = (0, r_{\infty}) \times (0, 2\pi)$. Thus we assume the separation of variables in r and θ , and set

$$\Psi_1 = \sum_{m=0}^N \psi_m(r) e^{im\theta}, \quad G = \sum_{m=0}^N \hat{G}_m(r) e^{im\theta}.$$

Substitution into the Helmholtz equation (3) then leads to the inhomogeneous Bessel equation in the radial direction for each azimuthal mode m ,

$$\partial_{rr} \psi_m + \frac{1}{r} \partial_r \psi_m - \left(\frac{m^2}{r^2} - k^2 \right) \psi_m = \hat{G}_m, \quad (4a)$$

where

$$\hat{G}_m(r) = \int_0^{2\pi} G(r) e^{-im\theta} d\theta$$

is the Fourier transformed inhomogeneous right-hand-side $G(r, \theta)$. Requiring that the scattered wave component be outward propagating is given by the radiation boundary condition at $r = r_{\infty}$,

$$\psi_m(r_{\infty}) = A_m H_m(kr_{\infty}), \quad (4b)$$

where H denotes the Hankel function of the first kind and A_m is a constant to be determined. In the limit $kr \gg 1$,

$$H_m(kr) = J_m(kr) + iY_m(kr) \approx \sqrt{\frac{2}{\pi kr}} e^{i(kr - \frac{1}{2}n\pi - \frac{1}{4}\pi)},$$

and thus may be interpreted as an outward propagating plane wave. The solution for $\psi_m(r)$ can be written in a closed analytical form

$$\psi_m(r) = B_m(r) J_m(kr) + C_m(r) Y_m(kr). \quad (5a)$$

J_m, Y_m are the Bessel functions of the first and second kind and the coefficients $A_m, B_m(r), C_m(r)$, are determined using a variational, or equivalently a Green-function, method to solve (4) together with regularity at the origin $r = 0$ as

$$\begin{aligned} A_m &= -i\frac{\pi}{2} \int_0^{r_\infty} J_m(ks) \hat{G}_m(s) s ds \\ B_m(r) &= -\frac{\pi}{2} \int_0^{r_\infty} (iH_m(ks) + Y_m(ks)) \hat{G}_m(s) s ds \\ C_m(r) &= \frac{\pi}{2} \int_0^r J_m(ks) \hat{G}_m(s) s ds. \end{aligned} \quad (5b)$$

5. NUMERICAL ALGORITHM

The solution for the wave distortion Ψ_1 may be computed by a direct numerical evaluation of the integrals for the variational coefficients (5b) by quadrature. However such a procedure is not used due to degradation of the numerical accuracy in the vicinity of the coordinate singularity $r = 0$; there Bessel functions of the second kind $Y_m \sim r^{-m}$ rapidly diverge to the floating point limit of the computer. Consequently, round-off errors, that violate the ordering of the perturbation scheme, occur in (5a) when forming products between algebraically diverging $Y_m \sim r^{-m}$ and converging $J_m \sim r^m$ quantities.

Round-off errors are avoided by selecting an appropriate choice of basis functions that are well-behaved at the coordinate singularity. We choose the set of Chebyshev polynomials, $\{T_j(r), j = 0, p\}$, because of their spectral characteristics on the stretched coordinates $r = \cos(\phi)$; namely $T_j(\phi) = \cos j\phi$. This allows the implementation of a spectrally accurate numerical scheme for generating the acoustic wave field (i.e., exponential convergence in accuracy as order $p \gg 1$). Additionally, the spectral representation utilizes the Fast-Fourier transform (FFT) in both the radial and azimuthal directions. Since Chebyshev polynomials are not the natural basis functions arising in the inhomogeneous Bessel equations, $\psi_m(r)$ must be determined by solving the boundary-value problem (4) together with a regularity condition at the coordinate singularity. However, we note that no regularity condition need be imposed if the computational domain is extended to the interval $(-r_\infty, r_\infty)$, therefore it follows from an inspection of (4) and (5) that the analytical solution $\psi_m(r)$ may be decomposed into linearly independent symmetric and antisymmetric radial parts according to whether m is even or odd. Therefore, for each order m , one need only impose the correctly symmetrised radiation boundary condition at $r = -\infty$ to ensure regularity at $r = 0$. On rescaling the radial interval to $(-1, 1)$, this gives,

$$\psi_m(-1) = (-1)^m \psi_m(1) = (-1)^m A_m H_m(k).$$

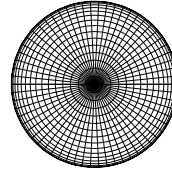


Figure 2. Collocation points for Fourier-Chebyshev grid in (r, θ) -space.

We thus employ the following spectral Fourier-Chebyshev decomposition on the extended domain $[-1, 1] \times [0, 2\pi)$

$$\begin{aligned} \Psi_1(r, \theta) &= \sum_{\substack{m,j \\ \text{even}}} \psi_{m,j} T_j(r) e^{im\theta} + \sum_{\substack{m,j \\ \text{odd}}} \psi_{m,j} T_j(r) e^{im\theta} \\ G(r, \theta) &= \sum_{\substack{m,j \\ \text{even}}} g_{m,j} T_j(r) e^{im\theta} + \sum_{\substack{m,j \\ \text{odd}}} g_{m,j} T_j(r) e^{im\theta}. \end{aligned}$$

Figure 2 illustrates a sample grid of collocation points in physical space. The spectral coefficients $\psi_{m,j}$ are determined by substituting the above expression into the boundary value problem (4) and solving the resulting system of linear algebraic equations together with the radiation boundary condition for each azimuthal order m , namely

$$\begin{aligned} L_{i,j} \psi_{m,j} &= g_{m,j} \\ \sum_{m,j} \psi_{m,j} &= A_m H_m(k) \end{aligned} \quad (6)$$

for $j = \text{either even or odd}$.

$L_{i,j}$ is a pentadiagonal matrix operator. The spectral coefficients $g_{m,j}$ are obtained from the inhomogeneous right-hand-side $G(r, \theta)$ by a two-dimensional FFT. To solve (6) we employ the “tau”-method where the algebraic equations for the highest Chebyshev mode in (6a) is neglected and exchanged with the boundary condition (6b). The so-called “tau”-errors arising from this operation are significantly small and always remain in the highest-order Chebyshev mode. Once all the spectral coefficients $\psi_{m,j}$ have been obtained the physical solution is determined by a two-dimensional inverse FFT to (r, θ) -space.

6. INVERSION

Having solved the forward problem of generating artificial acoustic wave fields, which suffer phase distortions due to the horizontal inhomogeneity $K(r, \theta)$ in the background atmosphere, we now seek a procedure to recapture $K(r, \theta)$ by analysing the wave field $\Psi(r, \theta)$. This requires a knowledge of the weak phase variation $\phi(r, \theta)$ in the wave field, which typically occur on lengthscales much greater than the characteristic wavelength of the wave field. However, it is not yet clear how to extract a two-dimensional phase variation. We therefore extend an inversion procedure first developed by Gough et al. (1991, 1992) for an analysis on one-dimensional acoustic wave-trains. The inversion procedure proposed is a

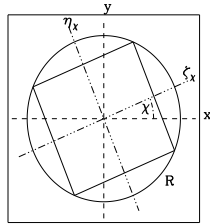


Figure 3. Computational domain R containing an example inscribed square within which lateral averages are performed along η_χ

four-step method which involves:

- a) computing an ensemble of one-dimensional wave-trains by performing an averaging of the two-dimensional wave field about selected propagation directions,
- b) extracting the averaged phase variations along these directions of propagation,
- c) inverting for the corresponding averaged inhomogeneity, and finally,
- d) performing a tomographic inversion on the ensemble of averaged inhomogeneities to reconstruct the two-dimensional background variation.

a) Lateral averaging

Given the circular computational domain R the wave field within an inscribed square subdomain is extracted for averaging (Figure 3). The orientation of the inscribed square is defined by the extent to which its cartesian axes ζ, η are rotated with respect to the upright x, y axes. The two coordinate systems are related by

$$\begin{pmatrix} \zeta_\chi \\ \eta_\chi \end{pmatrix} = \begin{pmatrix} \cos \chi & \sin \chi \\ -\sin \chi & \cos \chi \end{pmatrix} \begin{pmatrix} x \\ y \end{pmatrix},$$

where the χ denotes the angular orientation of the inscribed square. The following one-dimensional lateral average is then performed on the wave field $\Psi(\zeta_\chi, \eta_\chi)$ within the inscribed square,

$$\langle \Psi(\zeta_\chi) \rangle = \int_{square} \Psi(\zeta_\chi, \eta_\chi) d\eta_\chi$$

We postulate that such an averaged wave field contains information about the variation of the averaged background inhomogeneity along ζ_χ , i.e.,

$$\langle K(\zeta_\chi) \rangle = \int_{square} K(\zeta_\chi, \eta_\chi) d\eta_\chi.$$

We further postulate that an ensemble of averages taken on inscribed squares with angular orientation $0 \leq \chi < \pi$ contains all the information necessary to reconstruct the two-dimensional inhomogeneity $K(r, \theta)$. We define this ensemble average by $\langle K(\zeta; \chi) \rangle$

b) Hilbert inversion for the phase field.

Even though $\langle \Psi(\zeta_\chi) \rangle$ is a superposition of many simple wave components, we represent it by a singly averaged

wave

$$\langle \Psi(\zeta_\chi) \rangle = A(\zeta_\chi; \omega_*) \cos \phi(\zeta_\chi; \omega_*),$$

having variable amplitude $A(\zeta_\chi; \omega_*)$ and phase $\phi(\zeta_\chi; \omega_*)$. Recall that the frequency ω_* defines the depth $z = z_*$ of the atmosphere being sampled by the acoustic waves. The Hilbert transform of the averaged wave field $\langle \Psi(\zeta_\chi) \rangle$ is defined as

$$H[\langle \Psi(\zeta_\chi) \rangle] = \frac{1}{\pi} \text{P} \int_{-\infty}^{+\infty} \frac{\langle \Psi(\xi) \rangle}{\xi - \zeta_\chi} d\xi, \quad (7)$$

where P denotes the Principal part. The averaged wave field $\langle \Psi(\zeta_\chi) \rangle$ can formally be separated out into an amplitude and phase according to

$$\phi(\zeta_\chi) = -\tan^{-1} \left(\frac{H[\langle \Psi(\zeta_\chi) \rangle]}{\langle \Psi(\zeta_\chi) \rangle} \right),$$

$$A(\zeta_\chi)^2 = \langle \Psi(\zeta_\chi) \rangle^2 + H(\langle \Psi(\zeta_\chi) \rangle)^2.$$

Note that the Hilbert transform for a pure plane wave $\langle \Psi(\zeta_\chi) \rangle = A \cos(kx + \delta)$, with A, δ constant, is given by $H[\langle \Psi(\zeta_\chi) \rangle] = -A \sin(kx + \delta)$. Thus the above relation for the amplitude and phase follows trivially. Moreover, given that an arbitrary signal may be represented as a superposition of plane waves, this relation implies that the Hilbert transform of a signal may be computed trivially: one simply takes the FFT of the signal, multiply each of the Fourier coefficients by $e^{i\pi/2}$ (which is equivalent to the Hilbert transform of a plane wave), and then take the inverse FFT to real-space. To avoid corruption of the Hilbert transform by the Gibbs phenomenon occurring as consequence of taking the FFT of nonperiodic signals, the signal should be convolved with an appropriate windowing function. We implement a folding operation proposed by Isreali et al. 1993 which folds the tails of the signal such that the function and all of its even derivatives vanish at some newly defined endpoints (specified close to the original endpoints of the interval). The signal may then be extended periodically and its Hilbert transform may be computed accurately using the FFT.

c) Inversion for $\langle K(\zeta_\chi) \rangle$.

Provided that the variation in the wave number K varies on a scale much greater than K^{-1} , the laterally averaged $\langle K(\zeta_\chi) \rangle$ can validly be obtained from the JKWB approximation as

$$\langle K(\zeta_\chi) \rangle = \frac{d\langle \phi(\zeta_\chi) \rangle}{d\zeta_\chi} \quad \text{or} \quad \langle K(\zeta_\chi) \rangle = [A(\zeta_\chi)]^{-2}. \quad (8)$$

Gough et al. (1992, 1993) have shown that the most accurate results are obtained from the former expression (8a) involving the phase variations.

In Figure 4 we illustrate results of the inversion procedure b) and c) performed on various averaged wave fields $\langle \Psi(\zeta_\chi) \rangle$ to obtain the corresponding laterally averaged variations in the background inhomogeneity $\langle K(\zeta_\chi) \rangle$. These inversions (solid lines) were obtained from separate simulations of single distorted plane wave propagating at angle χ through the two-dimensional inhomogeneity given in Figure 1. It clearly can be seen that the inversion procedure utilizing Hilbert transforms is successful in recapturing the mean variations in the

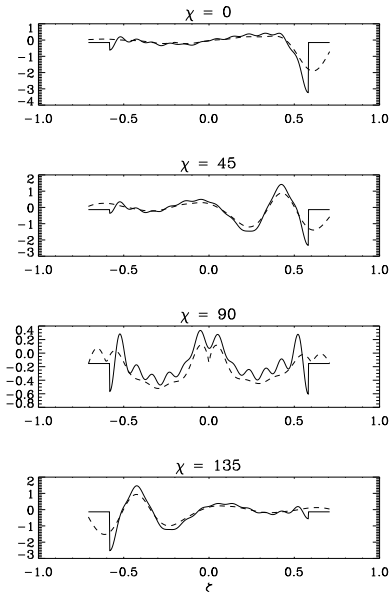


Figure 4. Sample inversions for mean variation, $\langle K(\zeta_\chi) \rangle / k - 1$ (solid line), in local wavenumber due to variations in sound speed c . The exact variation is given by the dashed line.

background from deduced phase variations. Note that information at the tails of the inversion is lost due to the folding operation used in computing the Hilbert transforms.

d) Tomographic reconstruction of $K(r, \theta)$

The ensemble $\langle K(\zeta; \chi) \rangle$ for all the averaged background inhomogeneity, obtained using the Hilbert inversion procedure, is the Radon transform of the original two-dimensional background inhomogeneity $K(r, \theta)$. That is, $\mathcal{R}K(r, \theta) = \langle K(\zeta; \chi) \rangle$,

where the symbol \mathcal{R} denoting the Radon transform is also called the *projection operator*. We now show that the Radon transform, which maps the spatial domain (r, θ) into the domain (ζ, χ) , contains all the information necessary to reconstruct $K(r, \theta)$. In the cartesian frame of the inscribed squares the Radon transform can be expressed as

$$\langle K(\zeta; \chi) \rangle = \int_{-\frac{1}{\sqrt{2}}}^{\frac{1}{\sqrt{2}}} K(\zeta \cos \chi - \eta \sin \chi, \zeta \sin \chi + \eta \cos \chi) d\eta$$

where $-1/\sqrt{2} \leq \zeta \leq 1/\sqrt{2}$, $0 \leq \chi < 2\pi$.

The quantity $\langle K(\zeta; \chi) \rangle$ is also called a *ray-sum*, since it represents the summation of $K(r, \theta)$ along a ray at a distance ζ within an inscribed square oriented at angle χ (see Figure 3). Note that in polar coordinates

$$\zeta = r \cos(\chi - \theta), \quad (9)$$

which implies that the Radon transform maps a fixed point in the physical space (r, θ) into a sinusoid in the (ζ, χ) domain. Conversely, the value of background inhomogeneity $K(r, \theta)$ at the fixed point (r, θ) is proportional to the accumulation of all the the ray-sums $\langle K(\zeta; \chi) \rangle$ along the sinusoid (9). This leads to the following definition for a *back-projection* operation \mathcal{B}

$$\mathcal{B}\langle K(r \cos(\chi - \theta); \chi) \rangle = \tilde{K}(r; \theta),$$

where

$$\tilde{K}(r; \theta) = \int_0^\pi \langle K(r \cos(\chi - \theta); \chi) \rangle d\chi$$

defines the back-projected Radon transform. It can be shown that this function is an image of the original background $K(r; \theta)$ blurred by the point-spread-function $1/|r|$ (Jain 1989). That is

$$\tilde{K}(r; \theta) = K(r; \theta) \odot \frac{1}{|r|},$$

where \odot denotes the convolution operation in polar coordinates. In particular, the back-projection operator \mathcal{B} is not the inverse of the \mathcal{R} , but is in fact its *adjoint* (Jain 1989). The two-dimensional variation $K(r; \theta)$ may then be recovered by first convolving the Radon transform with a spatial filter $h(r)$ whose response is $|r|$, which removes the blurring due to point-spread-function, followed by the back-projection operation. That gives the following inversion relation for the reconstruction of the two-dimensional variation

$$K(r, \theta) = \mathcal{B}\mathcal{R}[K(r, \theta) \odot h(r)],$$

which may written explicitly as

$$K(r; \theta) = \int_0^\pi \langle K(r \cos(\chi - \theta); \chi) \rangle \odot h(r) d\chi.$$

This inversion for the two-dimensional variation is obtained numerically by evaluating the right-hand-side using a quadrature that sums the convolved ray-sums along sinusoids.

Finally we note that this procedure for tomographic reconstruction, using Radon transforms and back-projections, normally demands that the object under investigation be unique and compact. However in the present case although it is true that the inscribed squares, from which Radon transform are computed, are compact their union does not define a unique object. The common intersection between the union of inscribed squares is an inscribed circle within the squares. To assess whether the back-projections recaptures the two-dimensional variation within this inscribed circle we perform a direct inversion (i.e. no oscillation data are used) on the variation $f(x, y)$ illustrated in Figure 1. In Figure 5a we illustrate the convolved Radon transform or one-dimensional averages computed from $K(r, \theta)$, and in Figure 5b we illustrate the reconstructed background. It can be seen that background variation is successfully reconstructed within an inscribed circle.

7. RESULTS AND DISCUSSION

An example of the two-dimensional inversion based the lateral averages $\langle K(\zeta; \chi) \rangle$ obtained from the N single wave inversion of Figure 4 with $k = 201$ is illustrated in Figure 6. It can be seen that the broadest aspects of the structure are captured. However, noise from the Hilbert inversion evident in Figure 4 contaminates the result. For wave fields consisting of a superposition of many plane monochromatic waves ($k = 201$) propagating in many directions, lateral averaging within inscribed squares results in modest contributions from those waves

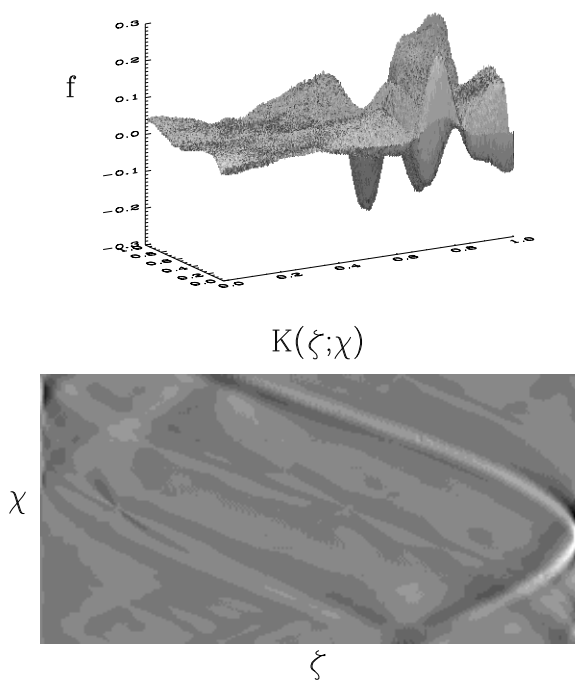


Figure 5. Tomographic reconstruction of background variation $f(x, y)$ given in Figure 1. a) (lower plot) Radon transform or lateral averages of $f(x, y)$. b) (Upper plot) Inversion by back-projection for two-dimensional variation.

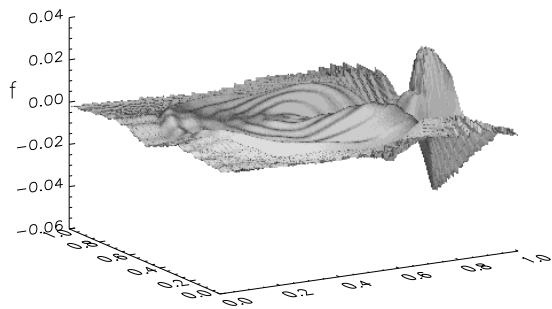


Figure 6. Tomographic inversion for the background variation $f(x, y)$, in Figure 1, using Radon transforms obtained from artificial wave data.

travelling at large angles to the propagation direction ζ . However, contributions from waves travelling along near parallel paths lead to interference effects that contaminate the envelope modulation in the averaged background (see example in Figure 7). For monochromatic waves such interference patterns have zero group velocity and therefore the spurious signals the contaminate the inversion cannot be swept out of the computational domain using a sequence of different time realisations of the wave field Ψ , as demonstrated by Gough et al (1992) for one-dimensional wave trains. It is found that some of the noise arising due to beating effects can be removed by spectral filtering (Julien, Gough & Toomre 1995), however, enough noise remains to dominate any attempts at inverting for the two-dimensional variation.

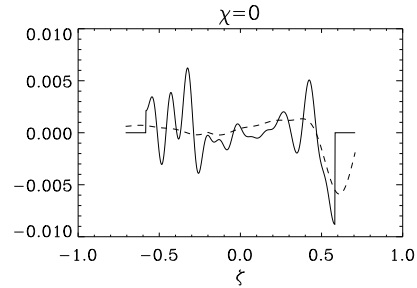


Figure 7. Sample mean variation $\langle K(\zeta_0) \rangle / k - 1$ in the averaged local wavenumber due to variations in sound speed c . The distorted wave field Ψ from which the average was computed contains 51 monochromatic waves with a random amplitudes and phases.

It therefore remains a key issue to devise a method that can account for the effects of mode beating within acoustic wave fields. If that were possible the procedures discussed in the paper would provide an inversion technique that will reveal three-dimensional subsurface thermal structures (that is two-dimensional horizontal structure as a function of depth). Such a technique will complement other local area helioseismic inversion methods such as ring diagrams which can only capture localised averages of an inhomogeneity as a function of depth.

This research was supported in part the Advanced Study Program at NCAR and by NASA through grants NAG5-2256 and NAS5-30396.

REFERENCES

1. Gough D.O., Merryfield W.J. and J. Toomre, 1991, in *Challenges to Theories of the Structure of Moderate Mass Stars*. Lecture Notes in Physics Vol. 288, ed. D.O. Gough, J. Toomre, Springer-Verlag p. 265
2. Gough D.O., Merryfield W.J. and J. Toomre, 1992, in *GONG 1992: Seismic Investigation of the Sun and Stars*, ASP Conf. Ser. Vol. 42, ed. T.M. Brown, Astron. Soc. Pac., p. 257
3. Isreali M., Vozovoi L. and A. Averbuch, 1993, *Spectral Multidomain Technique with Local Fourier Basis*. J. Comp. Phys. Vol. 8, No. 2, p. 125
4. Jain A.K. 1989, *Fundamentals of Digital Image Processing*, Prentice Hall.
5. Julien K.A., Gough D.O., and J. Toomre, 1994, in *GONG 1994: Helio- and Asteroseismology from the Earth and Space*, ASP Conf. Ser. Vol. 76, eds. R Ulrich, E. J. Rhodes, Jr., and W. Dappen, Astron. Soc. Pac., p. 196